Calculation of Resonances and Product State Distributions for the Unimolecular Dissociation of H_2S

Hong Zhang and Sean C. Smith*

Department of Chemistry, School of Molecular and Microbial Sciences,The University of Queensland, Qld 4072, Brisbane, Australia

Received: October 22, 2001; In Final Form: March 19, 2002

Resonance phenomena associated with the unimolecular dissociation of $H_2S \rightarrow SH + H$ have been investigated quantum mechanically by the Lanczos homogeneous filter diagonalization method using a newly developed potential energy surface (*J. Chem. Phys.* **2001**, *114*, 320). Resonance energies, widths (rates), and product state distributions have been obtained. Both dissociation rates and product state distributions of SH show strong fluctuations, indicating that the dissociation of H_2S is essentially irregular. Statistical analysis of neighboring level spacing and width distributions also confirms this behavior. The dissociation rates and product state distributions are compared to the predictions of quantum phase space theory.

1. Introduction

The study of unimolecular dissociation reactions is fundamentally important to many areas of pure and applied chemistry.[1,2] The quantum mechanical characterization of unimolecular dissociation involves the calculation of resonance states, which are quasi-bound, so-called compound states that are embedded in the continuum. These are eigenfunctions of the Schrödinger equation with outgoing wave boundary conditions. Because of the complex boundary conditions, the eigenvalues are necessarily complex, $\{E_R - i\Gamma/2\}$. The real part of the eigenvalue, E_R, is the energy of the metastable state of the molecule, whereas its unimolecular decay rate, k, is given in terms of the imaginary part, $\{\Gamma\}/\{\hbar\}$ (The latter relationship is only true if the resonance states are nonoverlapping.)[3] Unlike bound states, resonance states have a finite width in the energy domain and their wave functions extend to infinity. Because they are scattering states, resonances are generally more complicated to calculate than bound states. At present, it is possible to perform exact quantum mechanical calculations to obtain the energies and widths of the resonant states for only small molecules with a low density of states. Product state distributions reflect scattering from resonances into product states through a transition state, and thus contain additional clues about the intra- and intermolecular dynamics of the system. Each resonance has a unique width and is associated with a unique product state distribution. To fully understand unimolecular dissociation dynamics, therefore, it is useful to consider all three observables (energy, width, and product state distribution) for as many resonances as possible.

For large molecular systems, it is generally not possible to calculate resonances using exact quantum methods. Instead statistical theories such as Rice−Ramsperger−Kassel−Marcus (RRKM) theory[4,5] or phase space theory (PST)[6−8] are often used to estimate rate constant as well as product state distributions. Some statistical theories, which are based upon random matrix theory (RMT), can be used to describe the fluctuating behavior in the observables about the mean values.[9−12] It is interesting and informative to compare the results of exact quantum mechanical calculations with those of statistical theories for small molecules, and some very useful work has been done in this direction, mostly focusing on unimolecular dissociation of H_2CO, NO_2, and H_2O, using RMT and RRKM theory.[3,11−18] For example, Schinke et al.[18] have recently compared exact quantum dissociation rates in NO_2 with statistical theories and with experimental results. The multiexponential decay curves calculated by using quantum mechanical rates are in good agreement with the experimental curves, especially at longer times. The statistical adiabatic channel model can adequately describe the initial short time decay, but fails to predict the slow long time dissociation.

Recently, a new potential energy surface for H_2S has been developed,[19] which is based upon extensive ab initio calculations. The calculations have been performed for geometries sufficiently extended along the dissociative coordinates to allow the simulation of the dynamics in both entrance and exit channels accurately. A global representation of the lowest PES has been obtained by employing both the reproducing kernel Hilbert space (RKHS) method[20,21] and Murrell−Carter fitting scheme.[22] The RKHS method has proven successful in fitting the similar $H_2 + O$ (^1D) reaction. QCT calculations[23] have been performed on the new potential energy surface, and comparison of QCT results to the molecular beam experiments[24,25] shows general agreement. This potential energy surface has a deep well of about 3.9 eV and, therefore, a relatively high density of states. It is expected that the dissociation of H_2S will show statistical behavior; hence, the molecule is a good candidate for comparisons between exact quantum mechanical calculations (although these are difficult and challenging) and statistical approaches.

In this paper we will apply our recently developed Lanczos homogeneous filter diagonalization (LHFD) method[26] to the unimolecular dissociation of H_2S system. LHFD is a further

* To whom correspondence should be addressed. Fax: 61-7-3365-4299. E-mail: s.smith@chemistry.uq.edu.au.

10.1021/jp013919t CCC: $22.00
Published on Web 06/01/2002

simplified version of our previous Lanczos subspace filter diagonalization method.[27−30] In this Lanczos subspace method, we first transform the primary Hamiltonian into a Lanczos tridiagonal representation. We then perform filter diagonalization within the Lanczos representation to extract resonance energies and widths. Corresponding resonant eigenstates can be obtained within the Lanczos representation by an efficient three-term recursion, and then be utilized to obtain final state distributions in a manner described recently.[31] The paper is organized as follows. We describe the LHFD method in section 2. Then in section 3 we shall give the results of the quantum three-dimensional calculations performed on the unimolecular H_2S dissociation, alongside the statistical analysis and the comparison with PST results. Section 4 concludes this work.

2. Theoretical Methods

2.1 Resonance Energies and Widths. Quantum-mechanically, resonances can be treated in the time-independent domain by solving the homogeneous Schrödinger equation

$$(E - \hat{H}')\Psi_E = 0 \tag{1}$$

Here $\hat{H}' = \hat{H} - i\hat{V}_{abs}$, i.e., a complex absorbing potential augments the Hamiltonian ($\hat{H}$) to invoke the appropriate boundary conditions at "infinite" product separation, and Ψ_E is the resonance wave function. Briefly, in the LHFD method[26] we first project the augmented Hamiltonian into a Krylov subspace using the Lanczos method.[32] Inside the subspace, the Hamiltonian (represented as a tridiagonal matrix, T_M) can be used to perform FD calculations for various energy windows. Most FD approaches require the solution of inhomogeneous systems of linear equations, $Ax = b$, to converge filtered states. In contrast, our LHFD method, as its name suggests, relies upon solving $Ax = 0$. The advantage associated with this choice is that the linear system can be solved exactly by a simple scalar three-term recursion.[26]

In more detail, the LHFD algorithm for characterizing resonances can be summarized as follows:

(i) Choose a normalized, randomly generated initial vector $v_1 \neq 0$ and set β_1, $v_0 = 0$. Then use the 3-term Lanczos algorithm for complex-symmetric matrixes[33]

$$\beta_{k+1}v_{k+1} = \hat{H}'v_k - \alpha_k v_k - \beta_k v_{k-1} \tag{2}$$

to project the non-Hermitian augmented Hamiltonian into a Krylov subspace. The $M \times M$ tridiagonal representation of the Hamiltonian, T_M, has diagonal elements $\alpha_k = (v_k|\hat{H}|v_k)$ and subdiagonal elements $\beta_k = (v_{k-1}|\hat{H}|v_k)$. Note that a complex-symmetric inner product is used (i.e., bra vectors are not complex conjugated).

(ii) For all $j = 1, 2, ..., j_{max}$, generate filtered states $\phi(E_j)$ by solving the homogeneous linear system

$$(E_j - T_M)|\phi(E_j)\rangle = 0 \tag{3}$$

Here, a backward substitution recursion is employed:

(a) Choose ϕ_M, the M^{th} element of $\phi(E_j)$, to be arbitrary (but nonzero; usually set $\phi_M = 1$), and calculate

$$\phi_{M-1} = \frac{1}{\beta_M}(E_j\phi_M - \alpha_M\phi_M) \tag{4}$$

(b) For $k = M\text{-}1, M\text{-}2, ..., 2$, update scalar ϕ_{k-1}

$$\beta_k\phi_{k-1} = E_j\phi_k - \alpha_k\phi_k - \beta_{k+1}\phi_{k+1} \tag{5}$$

(iii) Construct the overlap matrix with elements $S_{jj'} = (\phi(E_j)|\phi(E_{j'}))$ and subspace Hamiltonian matrix with elements $W_{jj'} = (\phi(E_j)|T_M|\phi(E_{j'}))$. Note that $W_{jj'}$ can be calculated using a three-term summation

$$W_{jj'} = \sum_{k=1}^{M}[\phi_k(E_j)\beta_k\phi_{k-1}(E_{j'}) + \phi_k(E_j)\alpha_k\phi_k(E_{j'}) + \phi_k(E_j)\beta_{k+1}\phi_{k+1}(E_{j'})] \tag{6}$$

(iv) Solve the generalized complex-symmetric eigenvalue problem $WB = SB\epsilon$ to obtain the complex energies, $\{\epsilon\}$.

(v) Span the energy domain by repeating (ii)−(iv) window by window.

Due to the tridiagonal structure of the subspace Hamiltonian, one can generate *all* the elements of a filtered state by specifying practically any value for the scalar ϕ_M. Because the choice is arbitrary, the solution must be normalized after step (ii) to yield the true filtered state, $\phi(E_j) \leftarrow \eta_j \times \phi(E_j)$. To check the convergence of the eigenvalues as well as the quality of the eigenpairs generated by the above iterative methods, one can typically compute the error norm about the eigenenergy E

$$\sigma(E) = ||(T_M - E)\zeta(E)|| \tag{7}$$

where the Lanczos eigenvector $\zeta(E)$ is cheaply regenerated for each complex eigenenergy using eq 3. Clearly, true eigenvalues should have small error norms and can thus be distinguished from any unconverged/spurious eigenvalues.

2.2 Product State Distributions. The basic idea of asymptotic state analysis in unimolecular fragmentation has been proposed by Balint-Kurti et al. in the context of photodissociation,[34,35] and here we use it in the somewhat different context of resonance decay. The complex resonance wave functions in eq 1 obey the Siegert-type boundary conditions asymptotically, i.e., they are products of outgoing radial waves in the scattering coordinate, R, say, and internal eigenfunctions in the remaining coordinates. For our target system H_2S, the resonance wave function in terms of Jacobi coordinates (R, r, θ) has the following asymptotic form

$$\Psi_{E_R}(R_\infty,r,\theta) = \sum_n a_n(E_R)\sqrt{\frac{\mu_{H,SH}}{\hbar k_n}}e^{ik_nR_\infty}\varphi_n(r,\theta) \tag{8}$$

where

$$a_n(E_R) = \sqrt{\frac{\hbar k_n}{\mu_{H,SH}}}e^{-ik_nR_\infty}\langle\varphi_n(r,\theta)|\Psi_{E_R}(R_\infty,r,\theta)\rangle \tag{9}$$

and $n = (v, j)$ is product vibrational and rotational quantum number, and $k_n = \sqrt{2\mu_{H,SH}\hbar^{-2}(E_R - \epsilon_n)}$.

Within the subspace, we can use eq 8 to perform the asymptotic scattering analysis. The product rotational state distribution, $P_n = |a_n(E_R)|^2$, may be acquired by computing

$$P_n = \frac{\hbar k_n}{\mu_{H,SH}}|\langle\varphi_n(r,\theta)|\Psi E_R(R_\infty,r,\theta)\rangle|^2 \tag{10}$$

The analysis is done in the region where the interaction potential is small, but before the region where the absorbing potential is nonzero (where the resonance wave function is exponentially decreasing).

One can transform wave functions between the primary representation and the Lanczos subspace through

$$\zeta(E_R) = V^T \Psi E_R \tag{11}$$

$$\Psi E_R = V\zeta(E_R) = \sum_{i=1}^{M} \zeta_i(E_R)\upsilon_i \tag{12}$$

where $V = [\upsilon_1, \upsilon_2,...,\upsilon_M]$ is the column-orthonormal Lanczos vector matrix. So, using eq 12, the inner product appearing in eq 10 can be re-expressed[31]

$$\langle \varphi_n(r,\theta)|\Psi_{E_R}(R_\infty,r,\theta)\rangle = \sum_{i=1}^{M} \zeta_i(E_R)\langle \varphi_n(r,\theta)|\upsilon_i(R_\infty,r,\theta)\rangle = \sum_{i=1}^{M} \zeta_i(E_R)\chi_i^{(n)} \tag{13}$$

Thus, from a single Lanczos iteration sequence, one can calculate the complex resonance energies *and* the product state distributions for different resonances. This does not require that one construct the resonance wave functions explicitly in the primary representation because eqs 10 and 13 show that one need only compute and store the overlap coefficients $\chi_i^{(n)}$ as the iteration proceeds.

3. Calculations

3.1 Hamiltonian. The triatomic H_2S Hamiltonian with total angular momentum $J = 0$ is written in terms of product Jacobi coordinates

$$\hat{H} = -\frac{\hbar^2}{2\mu_{\mathrm{H,HS}}}\frac{1}{R}\frac{\partial^2}{\partial R^2}R - \frac{\hbar^2}{2\mu_{HS}}\frac{1}{r}\frac{\partial^2}{\partial r^2}r + \frac{\hbar^2}{2}\left(\frac{1}{\mu_{\mathrm{H,HS}}R^2} + \frac{1}{\mu_{\mathrm{HS}}r^2}\right)\hat{j}^2 + V(R,r,\theta) \tag{14}$$

where R is the separation of H from the center of mass of HS, r is the H−S separation, θ is the bend angle, and $\mu_{\mathrm{H,HS}}$ and μ_{HS} are reduced masses. This choice of product Jacobi coordinates facilitates the final state analysis for product state distributions via eqs 10 and 13. For $V(R,r,\theta)$ we utilize the newly developed ground-state H_2S PES by Zyubin et al.[19] The PES has an equilibrium geometry of $R_e = 2.53$ a_0, $r_e = 2.54$ a_0, and $\theta_e = 1.43$ rad and has a dissociation energy of 3.9 eV to the H + SH limit.

The Hamiltonian was then represented in a potential-optimized discrete variable representation[36] (PODVR). For the R coordinate, we used $N_R = 158$ PODVR points, which were contracted from 450 evenly spaced primitive Sinc DVR points[37] spanning the range from 0.5 a_0 to 15.5 a_0 with the one-dimensional reference potential $V(R,r_e,\theta_e)$. Similarly, for the r coordinate, $N_r = 142$ PODVR points were obtained from 426 primary DVR points spanning the range from 1.3 a_0 to 15.50 a_0 using the reference potential $V(R_e,r,\theta_e)$. For θ variable, we used $N_\theta = 43$ G-Legendre quadrature DVR points. The resulting direct product basis set was further contracted by discarding those points whose potential energies were higher than the cutoff energy $V_{\mathrm{cutoff}} = 1.2$ eV, resulting in the final basis size of 219030. Similar to our recent work,[38] we adopt the following empirical form for the absorbing potential in both R and r coordinates

$$\hat{V}_{\mathrm{abs}}(Z) = V_0\left\{\frac{Z - Z_0}{Z_{\max} - Z_0}\right\}^2 \tag{15}$$

where $Z_{\max} = 15.5$ a_0, and V_0 and $Z_{\max}$ are two adjusting parameters. For our purposes, we take $V_0 = 5.0$ eV and $Z_{\max} = 11.5$ a_0. One then has $\hat{H}_{\mathrm{abs}} = \hat{H} - i\hat{V}_{\mathrm{abs}}$.

The ro-vibrational eigenfunctions of HS are direct products

$$\varphi_n = \frac{1}{r}|\nu\rangle|j\rangle \tag{16}$$

where P_j is a Legendre polynomial of degree j. The j-dependent radial vibrational components satisfy the radial Schrödinger equation

$$\left[-\frac{\hbar^2}{2\mu_{\mathrm{HS}}}\frac{d^2}{dr^2} + \frac{j(j+1)\hbar^2}{2\mu_{\mathrm{HS}}r^2} + V_{\mathrm{HS}}(r)\right]|\nu\rangle = \epsilon_n|\nu\rangle \tag{17}$$

We take a slice of H_2S PES $V(R_\infty,r,\theta_e)$ as HS potential and use r PODVRs described above to solve eq 17 to get $|\nu\rangle$and ϵ_n.

3.2 Resonance Energies and Widths (Rates). Employing the method described above, we have computed resonance energies and widths window by window in the energy range from −0.02 eV to 0.28 eV. Here, the zero energy is referred to the second reaction threshold H_2 + S (^{1}D), but below about 0.28 eV the H_2 + S (^{1}D) channel is still not open due to zero-point vibrational energy, and in this paper we only consider the dissociation channel $H_2S \rightarrow SH + H$. In the LHFD approach, we set up a Lanczos subspace of order $M = 40\,000$, and stored the two sets of matrix elements $\{a_k\}_1^M$ and $\{\beta_k\}_2^M$ for subsequent construction of the subspace matrixes. Six energy windows of width 0.06 eV have been used, each with 200 basis functions, to perform the FD calculations. In Table 1 we present the calculated resonance energies and widths, together with corresponding error norms, just below the second reaction threshold. In this energy range, there are a total of 86 calculated narrow resonances, with their error norms less than 10^{-6}. Broader resonances cannot be extracted from the spectrum, simply because they are hidden in the background. In what follows, we will present some statistical analysis of the resonance energy level spacing and resonance width distribution, and compare the quantum rates with the results from statistical PST model.

In Figure 1, we present the nearest neighbor spacing distribution $P(s)$ of resonances after the spectrum was unfolded, i.e., rescaled to make the poles uniformly distributed with unit mean level spacing. Here, the spacing s is the distance of two complex eigenvalues in the complex plane. Also shown in this figure are the analogous Poisson distribution (long dashed line) and Ginibre distribution (short dashed line) for comparison. As pointed out elsewhere[17] (also see the references therein), the statistical analysis of bound states is different from that of resonances. For bound states, Wigner distribution corresponding to the eigenvalues of the random Gaussian ensemble of the orthogonal matrixes can be viewed as an evidence of the chaotic nature of the bound state spectrum, whereas the Poisson distribution corresponds to a regular bound state spectrum. On the other hand, for resonances, Ginibre distribution corresponds to the eigenvalues of the random Gaussian ensemble of the complex symmetric matrixes, thus can be used as an evidence of the chaotic nature of the spectrum, whereas the analogue

TABLE 1: Calculated Resonance Energies E_n and Widths Γ_n below the Second Reaction Threshold (H_2 + S (^{1}D))[a]

n	E_n	Γ_n	σ_n	n	E_n	Γ_n	σ_n
1	−0.0174	$.67 \times 10^{-03}$	$.36 \times 10^{-11}$	44	.1279	$.76 \times 10^{-02}$	$.31 \times 10^{-10}$
2	−0.0150	$.15 \times 10^{-01}$	$.49 \times 10^{-09}$	45	.1307	$.13 \times 10^{-02}$	$.61 \times 10^{-11}$
3	−0.0142	$.20 \times 10^{-02}$	$.15 \times 10^{-10}$	46	.1351	$.35 \times 10^{-03}$	$.39 \times 10^{-11}$
4	−0.0086	$.46 \times 10^{-03}$	$.44 \times 10^{-11}$	47	.1410	$.36 \times 10^{-03}$	$.48 \times 10^{-11}$
5	−0.0069	$.32 \times 10^{-02}$	$.59 \times 10^{-10}$	48	.1444	$.21 \times 10^{-02}$	$.15 \times 10^{-11}$
6	−0.0042	$.95 \times 10^{-03}$	$.42 \times 10^{-10}$	49	.1459	$.11 \times 10^{-01}$	$.78 \times 10^{-10}$
7	.0041	$.36 \times 10^{-02}$	$.21 \times 10^{-11}$	50	.1516	$.79 \times 10^{-02}$	$.11 \times 10^{-09}$
8	.0071	$.24 \times 10^{-02}$	$.13 \times 10^{-11}$	51	.1522	$.69 \times 10^{-03}$	$.90 \times 10^{-11}$
9	.0124	$.12 \times 10^{-03}$	$.29 \times 10^{-10}$	52	.1567	$.16 \times 10^{-02}$	$.22 \times 10^{-10}$
10	.0147	$.48 \times 10^{-02}$	$.11 \times 10^{-09}$	53	.1590	$.37 \times 10^{-02}$	$.18 \times 10^{-10}$
11	.0152	$.19 \times 10^{-02}$	$.17 \times 10^{-10}$	54	.1619	$.11 \times 10^{-02}$	$.15 \times 10^{-10}$
12	.0201	$.69 \times 10^{-03}$	$.35 \times 10^{-10}$	55	.1659	$.14 \times 10^{-02}$	$.88 \times 10^{-11}$
13	.0215	$.10 \times 10^{-01}$	$.15 \times 10^{-08}$	56	.1693	$.13 \times 10^{-02}$	$.90 \times 10^{-11}$
14	.0238	$.23 \times 10^{-03}$	$.17 \times 10^{-10}$	57	.1758	$.69 \times 10^{-03}$	$.95 \times 10^{-11}$
15	.0270	$.22 \times 10^{-02}$	$.11 \times 10^{-09}$	58	.1780	$.50 \times 10^{-02}$	$.41 \times 10^{-11}$
16	.0277	$.24 \times 10^{-03}$	$.11 \times 10^{-10}$	59	.1820	$.15 \times 10^{-02}$	$.38 \times 10^{-11}$
17	.0311	$.17 \times 10^{-03}$	$.55 \times 10^{-11}$	60	.1830	$.14 \times 10^{-01}$	$.19 \times 10^{-10}$
18	.0350	$.34 \times 10^{-02}$	$.86 \times 10^{-10}$	61	.1867	$.14 \times 10^{-02}$	$.64 \times 10^{-11}$
19	.0359	$.22 \times 10^{-03}$	$.90 \times 10^{-11}$	62	.1907	$.31 \times 10^{-02}$	$.20 \times 10^{-10}$
20	.0408	$.62 \times 10^{-02}$	$.67 \times 10^{-10}$	63	.1973	$.15 \times 10^{-02}$	$.34 \times 10^{-11}$
21	.0445	$.29 \times 10^{-03}$	$.14 \times 10^{-10}$	64	.1999	$.15 \times 10^{-02}$	$.33 \times 10^{-11}$
22	.0497	$.98 \times 10^{-03}$	$.38 \times 10^{-09}$	65	.2013	$.49 \times 10^{-02}$	$.74 \times 10^{-11}$
23	.0509	$.41 \times 10^{-02}$	$.21 \times 10^{-09}$	66	.2046	$.20 \times 10^{-03}$	$.67 \times 10^{-11}$
24	.0577	$.24 \times 10^{-02}$	$.19 \times 10^{-09}$	67	.2060	$.97 \times 10^{-02}$	$.31 \times 10^{-10}$
25	.0593	$.25 \times 10^{-01}$	$.11 \times 10^{-07}$	68	.2064	$.15 \times 10^{-03}$	$.57 \times 10^{-11}$
26	.0641	$.68 \times 10^{-02}$	$.64 \times 10^{-10}$	69	.2086	$.87 \times 10^{-03}$	$.25 \times 10^{-11}$
27	.0654	$.62 \times 10^{-02}$	$.51 \times 10^{-10}$	70	.2122	$.31 \times 10^{-03}$	$.76 \times 10^{-11}$
28	.0704	$.94 \times 10^{-03}$	$.30 \times 10^{-11}$	71	.2146	$.36 \times 10^{-01}$	$.97 \times 10^{-08}$
29	.0771	$.67 \times 10^{-03}$	$.90 \times 10^{-11}$	72	.2168	$.39 \times 10^{-02}$	$.32 \times 10^{-10}$
30	.0801	$.91 \times 10^{-02}$	$.54 \times 10^{-08}$	73	.2225	$.45 \times 10^{-03}$	$.16 \times 10^{-11}$
31	.0828	$.18 \times 10^{-02}$	$.28 \times 10^{-09}$	74	.2295	$.35 \times 10^{-02}$	$.67 \times 10^{-11}$
32	.0871	$.20 \times 10^{-02}$	$.13 \times 10^{-10}$	75	.2359	$.34 \times 10^{-02}$	$.91 \times 10^{-11}$
33	.0907	$.12 \times 10^{-02}$	$.12 \times 10^{-10}$	76	.2395	$.54 \times 10^{-02}$	$.75 \times 10^{-11}$
34	.0950	$.22 \times 10^{-03}$	$.73 \times 10^{-11}$	77	.2445	$.97 \times 10^{-03}$	$.11 \times 10^{-10}$
35	.1014	$.61 \times 10^{-03}$	$.14 \times 10^{-10}$	78	.2472	$.12 \times 10^{-02}$	$.22 \times 10^{-11}$
36	.1054	$.33 \times 10^{-02}$	$.61 \times 10^{-11}$	79	.2525	$.14 \times 10^{-01}$	$.25 \times 10^{-08}$
37	.1056	$.13 \times 10^{-01}$	$.63 \times 10^{-10}$	80	.2563	$.18 \times 10^{-02}$	$.30 \times 10^{-10}$
38	.1113	$.79 \times 10^{-03}$	$.34 \times 10^{-11}$	81	.2652	$.39 \times 10^{-02}$	$.46 \times 10^{-10}$
39	.1148	$.36 \times 10^{-03}$	$.49 \times 10^{-11}$	82	.2687	$.67 \times 10^{-04}$	$.13 \times 10^{-10}$
40	.1176	$.23 \times 10^{-01}$	$.42 \times 10^{-09}$	83	.2695	$.12 \times 10^{-02}$	$.50 \times 10^{-11}$
41	.1198	$.47 \times 10^{-03}$	$.48 \times 10^{-11}$	84	.2715	$.58 \times 10^{-02}$	$.46 \times 10^{-10}$
42	.1222	$.60 \times 10^{-03}$	$.22 \times 10^{-11}$	85	.2788	$.29 \times 10^{-02}$	$.38 \times 10^{-10}$
43	.1269	$.90 \times 10^{-03}$	$.45 \times 10^{-11}$	86	.2794	$.35 \times 10^{-02}$	$.48 \times 10^{-10}$

[a] Also shown are the corresponding error norms σ_n. The zero energy is referred to the second reaction threshold. All energy units are in EV.

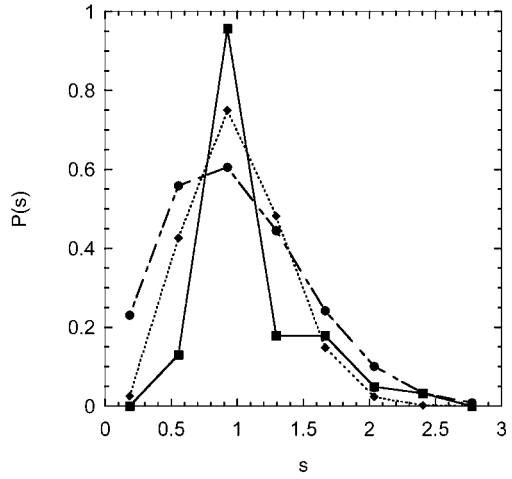

Figure 1. Plot of the nearest neighbor spacing distribution $P(s)$ of the unfolded spectrum for resonant states (solid line). The bin length is 0.37. Also shown in this figure are Poisson distribution (long dashed line) and Ginibre distribution (short dashed line) for comparison.

Poisson distribution, which is in fact identical to the Wigner distribution for bound states, corresponds to a regular quantum spectrum.[11,12,39] A superficial inspection reveals that the level spacing distribution obtained from our computations is closer to the Ginibre distribution than to the Poisson limit, particularly at lower level spacings. This would seem to imply largely irregular behavior in unimolecular dissociation of H_2S. The comparison is clearly not definitive, however. This may be due to the fact that the number of resonances in the energy range below the opening of the second channel SH + H is not large (see Table 1) which makes the statistics subject to fluctuation. It may also be due to the presence of some traces of regular dynamics.

Figure 2 presents the resonance width distribution $P(\Gamma)$ obtained from our computations together with a χ^2 distribution with 1 degree of freedom (dashed line), i.e., Porter−Thomas distribution. Here, resonance width Γ is rescaled so that the average value is one. This kind of distribution was first found in the classic work of Porter and Thomas[40] when studying neutron emission widths of heavy nuclei. Porter and Thomas pointed out that compound nucleus states are so complex that the nuclear decay matrix elements have a Gaussian distribution with zero mean, and thus, the decay rates exhibit this distribution. This distribution is in fact a member of the family of chi-squared distributions with ν degrees of freedom,[12] and the

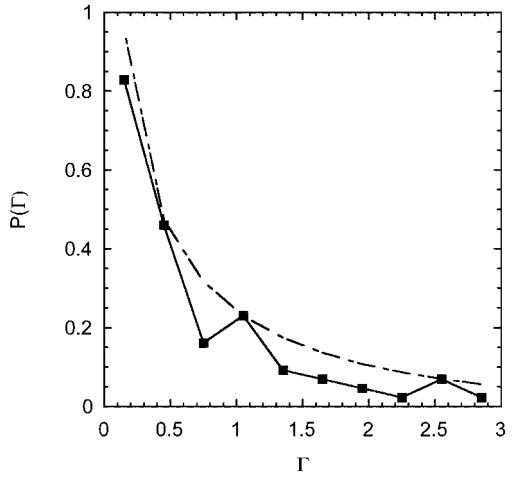

Figure 2. Resonance width distribution $P(\Gamma)$, with Γ rescaled such that $\langle\Gamma\rangle = 1$. The dashed line is a χ^2 distribution with 1 degree of freedom, i.e., Porter−Thomas distribution.

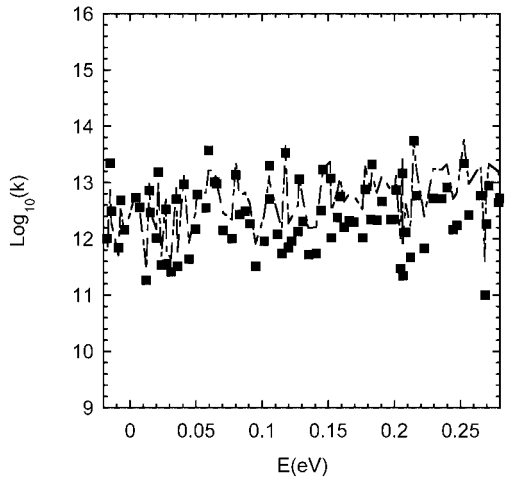

Figure 3. Plot of the logarithmic resonance rates, log (k), versus resonance energy in the energy range −0.02 eV to 0.28 eV. Solid squares represent the results from quantum LHFD calculations and dashed line denotes the statistical rates from quantum phase space theory. The unit of decay rate is s^{-1}.

number ν has been interpreted as the number of "effective" open decay channels. The fact that the Porter−Thomas distribution ($\nu = 1$) gives a reasonable fit is in some sense puzzling because the number of open channels in the SH + H arrangement is clearly greater than one over the energy range incorporated for the analysis (i.e., all resonances below the opening of the second arrangement channel). However, it should be borne in mind that the resonance density in this system is not so great that one can do a statistical analysis of resonances within a narrow energy range that has a well-defined number of open channels associated with it. Hence, although the comparison of Figure 2 is suggestive it cannot meaningfully be pushed too far.

For isolated resonances, the dissociation rates are widths divided by $\hbar$. In our considered energy range, most of the resonances are isolated since $\langle\Gamma_\rho\rangle = 0.906 < 1$, where $\rho(E)$ is the density of resonance states (see below). Only in several small regions are the resonances overlapping. Nevertheless, for simplicity, we will use the rates as defined above as quantum rates independent of the energy regime, following the work of Schinke et al.[15] In Figure 3 we present the quantum rates calculated from Table 1 (solid square), together the statistical rates from quantum phase space theory (dashed line). The quantum phase space theory[6−8] rate constant is given by

$$k_{\mathrm{PST}}(E) = \frac{W(E)}{h\rho(E)} \tag{18}$$

Here, $W(E)$ is the number of open product channels at energy E, $\rho(E)$ is the density of resonance states, and h is Planck's constant. Having obtained the resonance poles, the density of states $\rho(E)$ can be constructed quantum mechanically by summing over these poles[17]

$$\rho(E) = \sum_n \frac{\Gamma_n/2\pi}{(E - E_n)^2 + \Gamma_n^2/4} \tag{19}$$

Using the data in Table 1 the density of states in our considered energy range is easily calculated and then used to compute quantum PST rates. As can be seen from Figure 3, the dissociation rates acquired via LHFD and quantum PST are in good agreement. The dissociation rates show a large fluctuation, varied over 3 orders of magnitude. This fluctuating behavior has also been obtained by other theoretical calculations on HO_2 dissociation,[14,15,17] and observed experimentally for several dissociation systems including H_2CO, CH_3O, and NO_2.[41−43]

The close correspondence in the fluctuations of the quantum rate constants and the PST rate constants in this case should not be too surprising because we are utilizing the quantum density of states obtained directly from our computed resonances in the denominator of the PST expression, eq 18. If we had used energy-grain-averaged densities of states based on some zero-order Hamiltonian, as is commonly done for statistical calculations,[44] then, of course, the PST rate constants would not display the same fluctuations and would appear as a much smoother curve. Inspection of eq 19 reveals that the quantum density of states carries the signature of the quantum rate constants of the individual resonances. Indeed, when evaluated at the resonance energy E_n, $\rho(E_n)$ is precisely inversely proportional to Γ_n. Thus, in the present implementation it is the *denominator* of eq 18 which effectively guarantees the good agreement in Figure 3 between the fluctuating quantum rates and the PST rates. Because the characteristic which distinguishes PST from other statistical rate theories is the particular approximation which it invokes for the numerator of eq 18, Figure 3 should not be interpreted as a justification of the specific assumptions of PST for this molecular system. The appropriateness of PST in comparison with other more sophisticated statistical rate theories as approximations to the reaction flux (which relates to the numerator of eq 18, e.g., refs 14,15,45−49) becomes more relevant in the context of averages over resonances in the overlapping resonance regime of energies. This issue has been addressed in detail previously and so we do not pursue it further at this point.

3.3 Rotational State Distributions. As is evident from the form of eq 13, it proves to be relatively straightforward to calculate final rotational distributions for various resonant energies. Figure 4, parts a−d, shows the SH rotational distributions at four almost evenly spaced resonant energies. By inspecting Figure 4, we can identify some general features and trends. First, the number of occupied rotational channels increases steadily with energy, which is simply the result of energy conservation. Second, the distributions show a very complicated oscillatory behavior, with the number of oscillations generally increasing with energy. Third, the fluctuations in the distributions seem to be random and unpredictable from

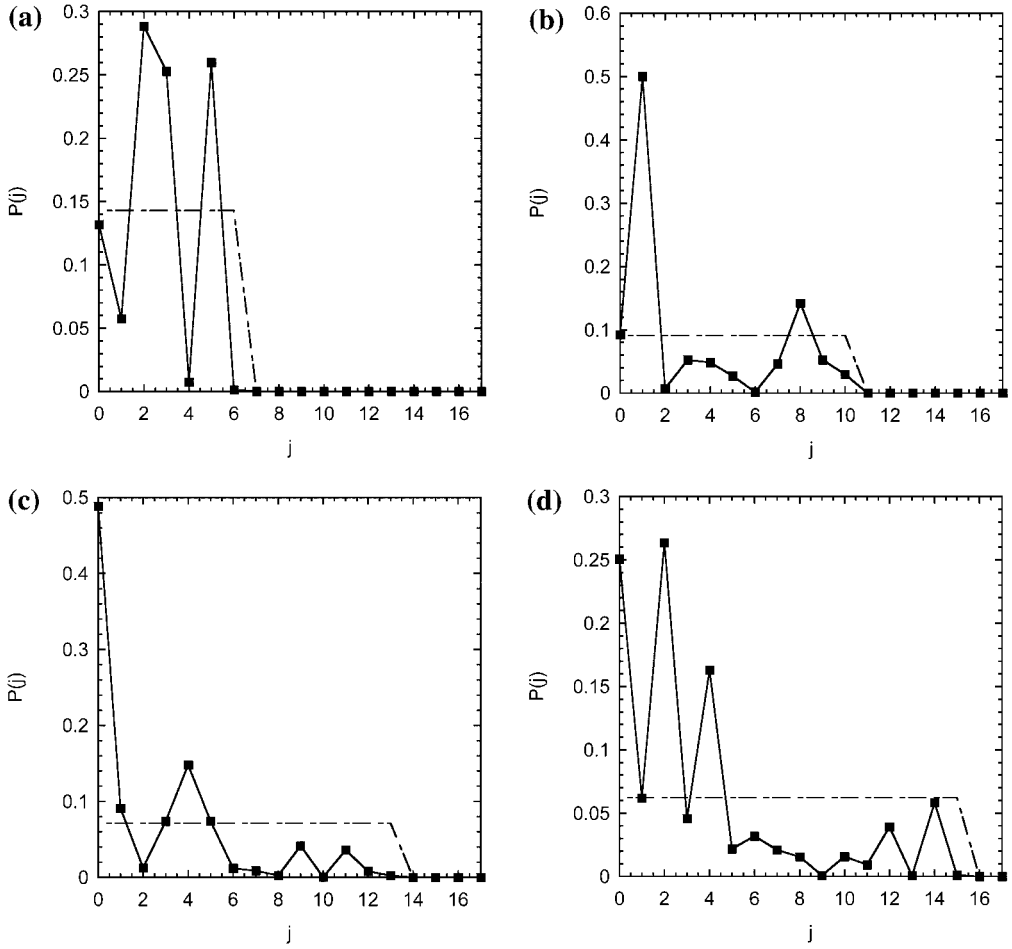

Figure 4. (a) SH ($v = 0$) rotational distributions at $E = 0.0311$ eV. Solid squares represent the results from quantum LHFD calculations, whereas dashed line denotes the statistical PST results. All distributions are normalized. (b) Same as previous figure, except $E = 0.113$ eV. Figure 4 (c). Same as previous figure, except $E = 0.1907$ eV. Figure 4 (d). Same as previous figure, except $E = 0.2687$ eV.

resonance to resonance. (We have calculated *all* the rotational state distributions for $v = 0$ for the resonances lying between -0.02 eV to 0.28 eV. For brevity, only four of them have been reported.) Fluctuations of this sort have been observed experimentally for NO rotational state distributions in the unimolecular dissociation of NO_2.[50,51]

The rotational state distributions of the fragments reflect the angular dependence of wave function at the translational state and the anisotropy of the PES in the exit channel. These distributions for the H_2S dissociation are complicated mainly due to the complicated translational-rotational coupling in the exit channel. In what follows, we will use a simple phase space statistical model to predict the product state distributions, and compare them with the quantum results. Phase Space Theory (PST) predicts that the amount of products formed in a particular ro-vibrational state is simply proportional to the ratio of the degeneracy of the particular ro-vibrational state to the total number of states which are accessible, while still conserving total energy and total angular momentum. At a particular energy, all product states with energies equal to or below it will be populated with equal probability. For the case of H_2S dissociation with total momentum $J = 0$, it predicts a constant distribution, i.e., all energy accessible rotational states will be equally populated. The PST product state distributions are also shown in Figure 4 (see dashed lines) for comparison. It is apparent that the fluctuations in the quantum distributions are not reproduced in the PST model. This in itself is not surprising since the simple assumptions of PST are not necessarily true in real molecular systems. What is of interest is whether the

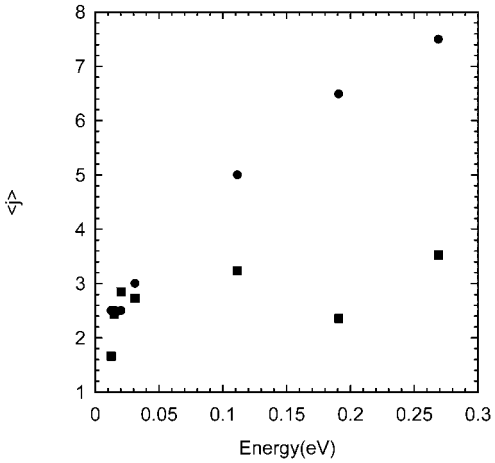

Figure 5. Average rotational excitation for both quantum (solid squares) and PST (solid circles) methods at the eight resonant energies $E = 0.0124$, 0.0147, 0.0152, 0.0201, 0.0311, 0.113, 0.1907, and 0.2687 eV.

average rotational distributions are in general agreement. Therefore, in Figure 5 we present the average rotational quantum number of the SH fragment for both quantum and PST methods at the eight selected resonance energies. At low energies, the general agreement between the two methods is satisfactory. However, with increasing energy the agreement becomes worse and worse, with PST apparently predicting hotter rotational distributions that are not born out by the quantum dynamical

calculations. This is partly because at low energies, the transition state is relatively loose, approximating that of PST. At higher energies, however, the variational transition state moves to shorter bond lengths such that the product state distributions depend more sensitively on dynamical interactions and the anisotropy of the potential surface in the exit channel past the transition state.[14,15,45,52]

4. Conclusion

In this paper, we have reported quantum mechanical calculations of the resonance states of H_2S dissociation using a Lanczos subspace filter diagonalization method. From a single set of Lanczos iterations, all the resonances *and* product state distributions have been efficiently obtained. In our considered energy range, most of the resonances are isolated ones. The resonance rate constants for dissociation show strong fluctuations, varied over 3 orders of magnitude. The rotational state distributions of SH show a complicated oscillatory behavior, with the number of oscillations generally increasing with energy. The oscillations vary from resonance to resonance in an unpredictable and random way. These results indicate there is an intricate coupling between the internal degrees of freedom in dissociation, and that the H_2S dissociation is largely irregular. Heuristic indicators of statistical behavior, such as statistical level-spacing and width distribution analyses, indicate that the H_2S dissociation appears to resemble statistical dissociation more than it does regular dissociation. Statistical quantum phase space theory has also been employed to estimate the dissociation rates and product state distributions. The comparison between quantum and statistical rates indicates quite good agreement at lower energies, including the dramatic fluctuations in the quantum rate constant. However, on closer inspection this agreement is seen to be due to the inclusion of the quantum density of states, eq 19, in the denominator of the microcanonical rate expression, eq 18, since the quantum density of states carries the signature of the fluctuating quantum resonance lifetimes. Because for this molecular system our energy range is essentially in the isolated resonance regime, further comparison with energy-grain-averaged PST is unlikely to yield additional information as the correctness or otherwise of the statistical decay postulate. Hence, we have not further pursued this line of comparison in this paper. The PST product state distributions do not agree well with the quantum results. The possible reasons for this failure are the PST assumption of an infinitely loose transition state and the neglect of the dynamical interactions within the exit channel.

Schinke et al.[1,53,54] have systematically investigated several triatomic systems such as HCO, HNO, and HO_2. The three systems typically represent the regular dissociation, mixed regular and irregular case, and the irregular one. From above analysis, the H_2S dissociation behaves between HNO and HO_2 systems, i.e., it is basically irregular, but there are discrepancies with statistical theories. Comprehensive experimental data which probe the resonances in the H_2S dissociation are still not available. The most likely approach would be photodissociation of the H_2S molecule in a supersonic jet which allows precise control of the total excitation energy and ensures that the total angular momentum is close to zero. The success of such an approach with single wavelength pumping would depend on the existence of an accessible electronically excited state which displays rapid internal conversion to the ground state. Other approaches involving stimulated emission pumping schemes may also possible; hence, one anticipates that such experimental data may well become available in the future for comparison with these and future calculations.

Acknowledgment. We are grateful to the University of Queensland, the Institute of Atomic and Molecular Sciences (Academia Sinica, Taipei, Taiwan), and the Australian Research Council for supporting this work. We would like to thank Professor Rex T. Skodje and Dr. Sheng Der Chao for provision of the H_2S PES code. We thank Professor Herschel Rabitz and Dr. Tak-San Ho for sending the RKHS fitting code. We also thank Dr. Anthony Rasmussen for assistance with the manuscript and Dr. Hua-Gen Yu for helpful discussions.

References and Notes

(1) Schinke, R.; Keller, H.-M.; Flothmann, H.; Stumpf, M.; Beck, C.; Mordaunt, D. H.; Dobbyn, A. J. *Adv. Chem. Phys.* **1997**, *101*, 745.
(2) Reid, S. A.; Reisler, H. *Annu. Rev. Phys. Chem.* **1996**, *47*, 495.
(3) Peskin, U.; Reisler, H.; Miller, W. H. *J. Chem. Phys.* **1994**, *101*, 9672.
(4) Marcus, R. A. *J. Chem. Phys.* **1952**, *20*, 359.
(5) Marcus, R. A.; Rice, O. K. *J. Phys. Colloid Chem.* **1951**, *55*, 894.
(6) Pechukas, P.; Light, J. C. *J. Chem. Phys.* **1965**, *42*, 3285.
(7) Pechukas, P.; Light, J. C.; Rankin, C. *J. Chem. Phys.* **1966**, *44*, 794.
(8) Klots, C. E. *J. Phys. Chem.* **1971**, *75*, 1526.
(9) Brody, T. A.; Flores, J.; French, J. B.; Mello, P. A.; Pandey, A.; Wong, S. S. M. *Rev. Mod. Phys.* **1981**, *53*, 385.
(10) Levine, R. D. *Adv. Chem. Phys.* **1988**, *70*, 53.
(11) Polik, W. F.; Moore, C. B.; Miller, W. H. *J. Chem. Phys.* **1988**, *89*, 3584.
(12) Polik, W. F.; Guyer, D. R.; Miller, W. H. *J. Chem. Phys.* **1990**, *92*, 3471.
(13) Waite, B. A.; Miller, W. H. *J. Chem. Phys.* **1980**, *73*, 3713.
(14) Dobbyn, A. J.; Stumpf, M.; Keller, H.-M.; Hase, W. L.; Schinke, R. *J. Chem. Phys.* **1995**, *102*, 586.
(15) Dobbyn, A. J.; Stumpf, M.; Keller, H.-M.; Schinke, R. *J. Chem. Phys.* **1996**, *104*, 8357.
(16) Someda, K.; Nakamura, H.; Mies, F. H. *Prog. Theor. Phys.* **1994**, *116*, 443.
(17) Mandelshtam, V. A.; Grozdanov, T. P.; Taylor, H. S. *J. Chem. Phys.* **1995**, *103*, 10 074.
(18) Kirmse, B.; Abel, B.; Schwarzer, D.; Grebenshchikov, S. Y.; Schinke, R. *J. Phys. Chem.* **2000**, *104*, 10 398.
(19) Zyubin, A. S.; Mebel, A. M.; Chao, S. D.; Skodje, R. T. *J. Chem. Phys.* **2001**, *114*, 320.
(20) Hollebeek, T.; Ho, T. S.; Rabitz, H. *Annu. Rev. Phys. Chem.* **1999**, *50*, 537.
(21) Ho, T.-S.; Hollebeek, T.; Rabitz, H.; Harding, L. B.; Schatz, G. C. *J. Chem. Phys.* **1996**, *105*, 10472.
(22) Murrell, J. N.; Carter, S. *J. Phys. Chem.* **1984**, *88*, 4887.
(23) Chao, S. D.; Skodje, R. T. *J. Phys. Chem. A* **2001**, *105*, 2474.
(24) Lee, S. H.; Liu, K. *Chem. Phys. Lett.* **1998**, *290*, 323.
(25) Lee, S. H.; Liu, K. *J. Phys. Chem. A* **1998**, *102*, 8637.
(26) Zhang, H.; Smith, S. C. *Phys. Chem. Chem. Phys.* **2001**, *3*, 2282.
(27) Yu, H. G.; Smith, S. C. *Ber. Bunsen-Ges. Phys. Chem.* **1997**, *101*, 400.
(28) Yu, H. G.; Smith, S. C. *J. Chem. Phys.* **1997**, *107*, 9985.
(29) Yu, H. G.; Smith, S. C. *Chem. Phys. Lett.* **1998**, *283*, 69.
(30) Yu, H. G.; Smith, S. C. *J. Comput. Phys.* **1998**, *143*, 484−494.
(31) Zhang, H.; Smith, S. C. *J. Chem. Phys* **2001**, *115*, 5751.
(32) Lanczos, C. *J. Res. Natl. Bur. Stand.* **1950**, *45*, 255.
(33) Moro, G.; Freed, J. H. *J. Chem. Phys.* **1981**, *74*, 3757.
(34) Balint-Kurti, G. G.; Dixon, R. N.; Marston, C. C. *J. Chem. Soc., Faraday Trans.* **1990**, *86*, 1741.
(35) Balint-Kurti, G. G.; Dixon, R. N.; Marston, C. C. *Int. Rev. Phys. Chem.* **1992**, *11*, 317.
(36) Echave, J.; Clary, D. *Chem. Phys. Lett.* **1992**, *190*, 225.
(37) Colbert, D. T.; Miller, W. H. *J. Chem. Phys.* **1992**, *96*, 1982.
(38) Zhang, H.; Smith, S. C. *J. Chem. Phys.* **2002**, *116*, 2354.
(39) Zimmermann, T.; Cederbaum, L. S.; Meyer, H. D.; Koppel, H. *J. Phys. Chem.* **1987**, *91*, 4446.
(40) Porter, C. E.; Thomas, R. G. *Phys. Rev.* **1956**, *104*, 483.
(41) Geers, A.; Kappert, J.; Temps, F.; Wiebrecht, J. W. *J. Chem. Phys.* **1993**, *99*, 2271.
(42) Miller, W. H.; Hernandez, R.; Moore, C. B.; Polik, W. F. *J. Chem. Phys.* **1990**, *93*, 5657.
(43) Reid, S. A.; Reisler, H. *J. Phys. Chem.* **1996**, *100*, 474.
(44) Gilbert, R. G.; Smith, S. C. *Theory of Unimolecular and Recombination Reactions*; Blackwell Scientific Publishers: Oxford, 1990.
(45) Song, K.; Peslherbe, G. H.; Hase, W. L.; Dobbyn, A. J.; Stumpf, M.; Schinke, R. *J. Chem. Phys.* **1995**, *103*, 8891.
(46) Wardlaw, D. M.; Marcus, R. A. *Adv. Chem. Phys.* **1988**, *70*, 231.

(47) Smith, S. C. *J. Chem. Phys.* **1992**, *97*, 2406.
(48) Smith, S. C. *J. Chem. Phys.* **1999**, *111*, 1830−1842.
(49) Truhlar, D. G.; Garrett, B. C.; Klippenstein, S. J. *J. Phys. Chem.* **1996**, *100*, 12 771.
(50) Robra, U.; Zacharias, H.; Welge, K. H. *Z. Phys. D* **1990**, *16*, 175.
(51) Miyawaki, J.; Yamanouchi, K.; Tsuchiya, S. *J. Chem. Phys.* **1993**, *99*, 254.
(52) Bergeat, A.; Cartechini, L.; Balucani, N.; Capozza, G.; Phillips, L. F.; Casavecchia, P.; Volpi, G. G.; L, L. B.; Rayez, J. C. *Chem. Phys. Lett.* **2000**, *327*, 197.
(53) Stumpf, M.; Dobbyn, A. J.; Mordaunt, D. H.; Keller, H.-M.; Fluethmann, H.; Schinke, R. *Faraday Discuss.* **1995**, *102*, 193.
(54) Schinke, R.; Keller, H.-M.; Stumpf, M.; Dobbyn, A. J. *J. Phys. B* **1995**, *28*, 3081.